European Journal of Radiology 120 (2019) 108654

Contents lists available at ScienceDirect

European Journal of Radiology

journal homepage: www.elsevier.com/locate/ejrad

Using CT texture analysis to differentiate cystic and cystic-appearing odontogenic lesions

Masafumi Oda[a,d], Pedro V. Staziaki[a], Muhammad M. Qureshi[a,b], V. Carlota Andreu-Arasa[a], Baojun Li[a], Koji Takumi[a,e], Margaret N. Chapman[a], Albert Wang[a], Andrew R. Salama[c,f], Osamu Sakai[a,b,c,*]

[a] Department of Radiology, Boston Medical Center, Boston University School of Medicine, United States
[b] Deparment of Radiation Oncology, Boston Medical Center, Boston University School of Medicine, United States
[c] Deparment of Otolaryngology – Head and Neck Surgery, Boston Medical Center, Boston University School of Medicine, United States
[d] Division of Oral and Maxillofacial Radiology, Kyushu Dental University, Kitakyushu, Fukuoka, Japan
[e] Department of Radiology, Kagoshima University Graduate School of Medical and Dental Sciences, Kagoshima, Japan
[f] Department of Oral & Maxillofacial Surgery, Boston Medical Center, Boston University Henry M. Goldman School of Dental Medicine, United States

ARTICLE INFO

Keywords:
CT
Texture analysis
Jaw lesions
Dentigerous cysts
Odontogenic keratocysts
Ameloblastomas

ABSTRACT

Purpose: Cystic and cystic-appearing odontogenic lesions of the jaw may appear similar on CT imaging. Accurate diagnosis is often difficult although the relationship of the lesion to the tooth root or crown may offer a clue to the etiology. The purpose of this study was to evaluate CT texture analysis as an aid in differentiating cystic and cystic-appearing odontogenic lesions of the jaw.

Methods: This was an IRB-approved retrospective study including 42 pathology-proven dentigerous cysts, 37 odontogenic keratocysts, and 19 ameloblastomas. Each lesion was manually segmented on axial CT images, and textural features were analyzed using an in-house-developed Matlab-based texture analysis program that extracted 47 texture features from each segmented volume. Statistical analysis was performed comparing all pairs of the three types of lesions.

Results: Pairwise analysis revealed that nine histogram features, one GLCM feature, three GLRL features, two Laws features, four GLGM features and two Chi-square features showed significant differences between dentigerous cysts and odontogenic keratocysts. Four histogram features and one Chi-square feature showed significant differences between odontogenic keratocysts and ameloblastomas. Two histogram features showed significant differences between dentigerous cysts and ameloblastomas.

Conclusions: CT texture analysis may be useful as a noninvasive method to obtain additional quantitative information to differentiate cystic and cystic-appearing odontogenic lesions of the jaw.

1. Introduction

Precise pre-operative differentiation between the different cysts and cystic-appearing tumors of the jaw is paramount as certain lesions may recur after enucleation and partial jaw resection is sometimes required for cure [1,2]. CT imaging is often requested for more definitive characterization of cystic lesions of the jaw incidentally identified on panoramic radiographs [3]. These lesions may also be encountered as incidental findings on CT examinations performed for other reasons and may present a diagnostic dilemma for the radiologist as the CT imaging characteristics of dentigerous cysts (DCs), odontogenic keratocysts (OKCs), and ameloblastomas (AMs) can be similar [4]. For example, large DCs can develop undulating borders, OKCs can be unilocular with a smooth border or can show an aggressive growth pattern including cortical expansion and root resorption, and AMs can be confused with large OKCs [5–7]. Additionally, the unicystic variant of AMs often associated with the crown may mimic DCs [5,8].

Texture analysis is a new quantitative imaging analysis that

Abbreviations: AM, ameloblastoma; DC, dentigerous cyst; OKC, odontogenic keratocyst; GLCM, gray-level co-occurrence matrix; GLN, gray-level nonuniformity; GLRL, gray-level run-length; HR, hazard ratio; HU, hounsfield units; RLN, run-length nonuniformity; SRE, short-run emphasis; SRLGE, short-run low gray-level emphasis

* Corresponding author at: Department of Radiology, Boston Medical Center, Boston University School of Medicine, FGH Building, 3rd Floor, 820 Harrison Avenue, Boston, MA, 02118, United States.
E-mail address: osamu.sakai@bmc.org (O. Sakai).

https://doi.org/10.1016/j.ejrad.2019.108654
Received 20 May 2019; Received in revised form 16 August 2019; Accepted 26 August 2019

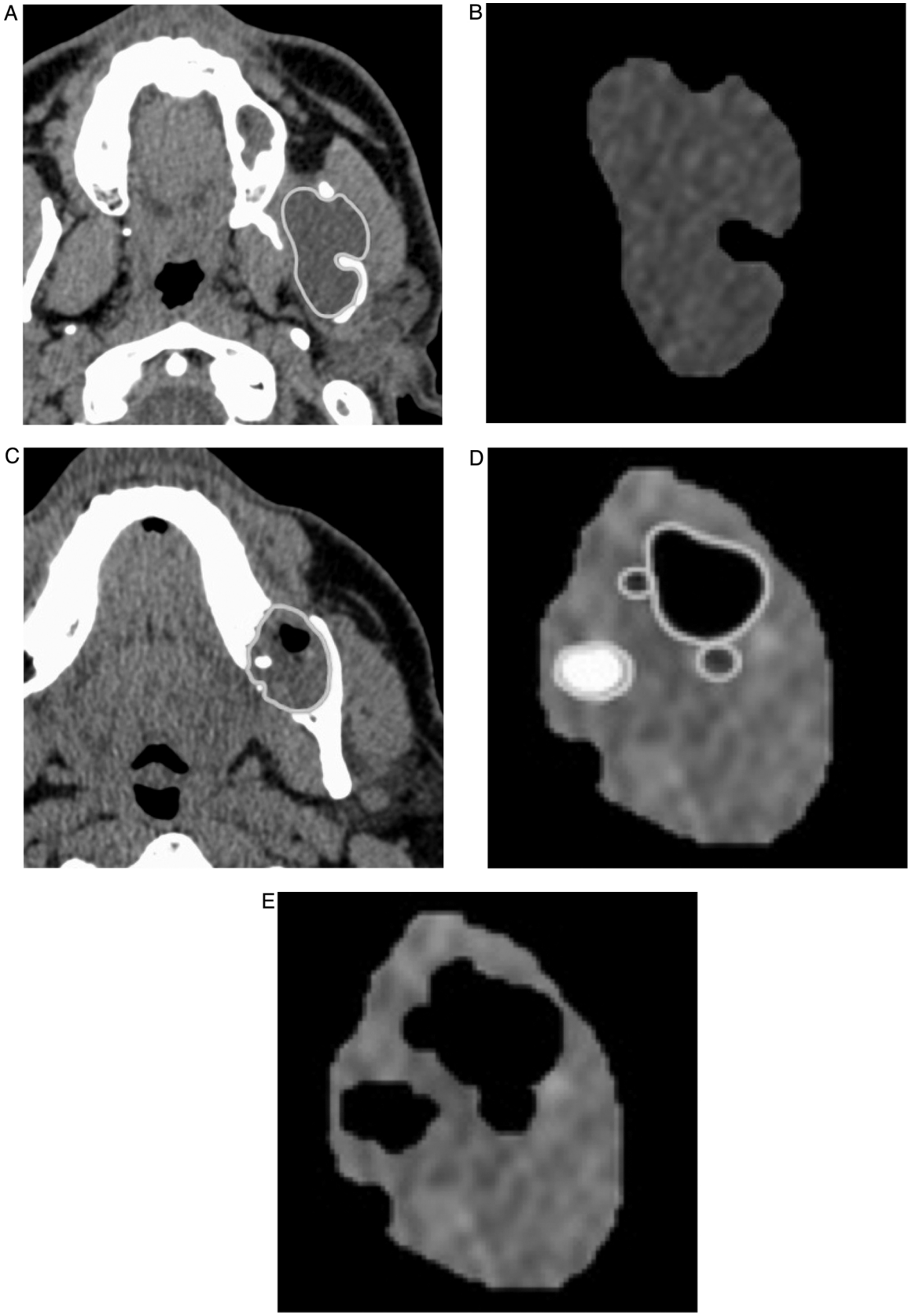

Fig. 1. Segmentation process. The lesions (*A* and *C*) were manually segmented not to include peripheral bone and septum (*A*) and masked the outside of the lesion (*B* and *D*) using OsiriX (Pixmeo SARL, Bernex, Switzerland). Areas of air-density and tooth with in the lesions (*C*) were manually segmented (*D*) and excluded (*E*). The texture features of segmented images (*B* and *E*) were analyzed.

ultimately provides a quantitative means of extracting image features that are useful for comparative analyses. Texture analysis has been reported to improve diagnostic accuracy and prediction of prognosis [9–13], and can be used to develop computational models using advanced machine learning algorithms that may serve as a tool for precision diagnosis and treatment [14]. Image texture on CT is defined as the pattern of variation in voxel intensity levels in an image. Texture analysis is a post-processing tool that allows the mathematic detection of subtle spatial arrangement of gray levels among adjacent pixels by extracting information native to image data, most of which are not perceived by the human eye [15,16]. In the past several years, CT texture analysis has been investigated in oncologic imaging as a surrogate for intra-tumoral heterogeneity to predict treatment outcome in patients with non-small cell lung cancer, hepatocellular carcinoma, colorectal cancer, and metastatic renal cell carcinoma [17–19]. Texture analysis has been utilized in the head and neck in detecting carcinoma, for the diagnosis of nodal metastases, HPV status, and for predicting local failure in chemoradiotherapy [20–24]. However, there is a dearth of research on texture analysis regarding cysts and cystic-appearing lesions of the jaw. We hypothesized that CT texture analysis can detect subtle differences of the intralesional feature among cystic and cystic-appearing lesions.

The purpose of this study was to evaluate the utility of CT texture features in distinguishing common cystic and cystic-appearing lesions of the jaw such as DCs, OKCs, and AMs.

2. Materials and methods

2.1. Patients

This retrospective study was approved by the institutional review board and the requirement to obtain written informed consent was waived. Retrospective search through our electronic medical records was performed to identify patients with pathologically proven DCs, OKCs without Gorlin syndrome and AMs who underwent pre-treatment CT examinations between January 2003 and July 2017. A total of 158 patients with DCs ($n = 64$), OKCs without Gorlin syndrome ($n = 59$), and AMs ($n = 43$) were identified. Patients who underwent a contrast enhanced CT were excluded. Imaging slices with severe artifact were excluded due to difficulty in calculating reliable texture parameters. Additionally, patients with very small lesions (not seen on greater than four contiguous 1.25 mm axial images) were excluded due to difficulty in performing an accurate manual contour on tumors below this size. We excluded 22 out of the 64 dentigerous cysts: nine lesions due to intravenous contrast administration, six lesions due to significant artifact, and seven lesions due to very small size. We excluded 22 out of the 59 OKCs and 24 of the 43 AMs: 15 OKCs and 20 AMs due to intravenous contrast administration, 4 OKCs and 2 AMs due to significant artifacts, and 3 OKCs and 2 AMs due to very small size. The remaining 42 DCs (24 men, 12 women [3 men and 3 women had 2 DCs]; age 6–82 years; median age, 49 years), 37 OKCs (20 men, 16 women [one man had 2 OKCs]; age 12–79 years; median age, 29 years) and 19 AMs (6 men, 13 women; age 17–85 years; median age, 43 years) were enrolled in this study.

2.2. CT imaging protocol

Non-contrast enhanced CT examinations were performed on 64-detector row CT scanners (Lightspeed VCT; GE Healthcare, Milwaukee, Wisconsin) with 120 kV, 225 mA and 1 s/rotation, and 1.25 mm thick images were reconstructed using soft tissue and bone algorithms per our institutional clinical protocol. Axial 1.25 mm images in soft tissue algorithm reconstruction were used for this analysis.

2.3. Qualitative analysis of the lesions

Characteristics of the lesions were qualitatively assessed by an oral and maxillofacial radiologist with 10 years of experience regarding lesion location, presence or absence of tooth crown, and presence or absence of septum.

2.4. Image segmentation and texture analysis

The lesion was manually contoured by an oral and maxillofacial radiologist with 10 years of experience blinded to the patient history. Segmentation of the lesion was performed using OsiriX (Pixmeo SARL, Bernex, Switzerland) on each axial image which includes the lesion not to include peripheral bone or septum. Also, regions of air-density and teeth within the lesion were excluded (Fig. 1). When severe streak artifacts within the lesion were seen, we excluded the slice with artifact and used only artifact-free slices for the texture analysis. Slices with a segmentation smaller than 100 pixels were also excluded.

Following manual segmentation, an in-house-developed Matlab (MathWorks, Natick, Massachusetts) texture analysis software extracted 47 texture features from each segmented volume [20,25]. The mean value of the textural features on an ROI basis was estimated. The volume of each primary lesion was also calculated. The 47 features included: 15 histogram features, 5 Gy-level co-occurrence matrix (GLCM) features, 11 Gy-level run-length (GLRL) features, 4 Gy-level gradient matrix (GLGM) features, 10 Laws features and 2 Chi-square features. Discussion on the extraneous math behind each texture feature in detail is in a subsequent On-line Appendix [15,16,20,25–28].

2.5. Statistical analysis

Texture features were compared by Kruskal-Wallis nonparametric analysis. Then the differences between all pairs of DCs, OKCs and AMs were analyzed using Mann-Whitney's U test for texture features with the significant difference in the Kruskal-Wallis test. The false discovery rate (FDR)-corrected P values (term Q values) were calculated in addition to raw P values to adjust for multiple comparisons. Statistical computations were performed using SAS 9.1.3 software (SAS Institute, Cary, NC). A P value $< .05$ was considered statistically significant.

3. Results

3.1. Characteristics of lesions

The characteristics of lesions and segmented volumes included in

Table 1
Characteristics of lesions and segmented volume.

	Dentigerous cyst	Odontogenic keratocyst	Ameloblastoma
Region			
Maxillary anterior	4	3	1
Maxillary posterior	6	10	–
Mandibular anterior	1	3	8
Mandibular posterior	31	21	10
Tooth within the lesion			
Present	42	14	4
Absent	–	23	15
Septum			
Present	–	11	11
Absent	42	26	8
Segmented Volume (cm^3)			
Average	2.65	5.36	5.18
Standard deviation	4.83	5.52	8.79
Median	0.52	3.94	1.2
Maximum value	21.8	23.7	35.6
Minimum value	0.062	0.176	0.083

Table 2
The values of texture features and results of Kruskal-Wallis nonparametric analysis.

	Dentigerous cyst		Odontogenic keratocyst		Ameloblastoma		Kruskal-Wallis test	
Texture features	Mean	SD	Mean	SD	Mean	SD	*P*-value	*Q*-value
Histogram features								
Mean	1072.42	16.80	1035.80	170.11	1021.68	243.47	**0.01***	0.071
Median	1072.03	16.39	1035.43	170.06	1021.26	243.45	**0.009***	0.071
SD	22.13	10.45	17.46	5.06	18.17	4.82	**0.02***	0.071
Entropy	5.90	0.29	5.80	0.32	5.75	0.28	0.094	0.143
2nd SD	10.55	4.61	8.55	2.34	8.61	2.32	**0.049***	0.109
Range	31.25	13.60	25.35	6.94	25.52	6.96	0.051	0.109
SD5	13.83	7.05	10.93	2.91	10.79	2.83	**0.019***	0.071
SD9	15.49	5.48	12.97	3.69	12.35	2.87	0.057	0.117
Geometric mean	1073.05	17.60	1036.20	170.71	1022.04	244.09	**0.011***	0.071
Harmonic mean	1072.77	17.40	1035.92	171.47	1021.70	244.81	**0.011***	0.071
IQR	28.60	9.96	22.48	6.69	22.90	5.33	**0.004***	0.071
Fourth moment	5.47e7	3.24e8	7.76e5	1.42e6	7.28e5	1.03e6	**0.025***	0.073
Test	0.54	0.11	0.51	0.08	0.56	0.10	0.060	0.118
Skewness	0.39	0.42	0.46	0.39	0.42	0.41	0.662	0.703
Kurtosis	4.06	2.17	4.03	1.53	3.90	1.37	0.894	0.894
GLCM features								
Entropy	0.90	0.40	1.14	0.41	0.95	0.48	**0.019***	0.071
Contrast	39.25	12.70	34.93	12.83	39.39	16.32	0.247	0.341
Correlation	0.72	0.08	0.71	0.07	0.70	0.08	0.765	0.782
Energy	5.52e-3	2.30e-3	4.96e-3	1.93e-3	5.85e-3	2.18e-3	0.226	0.322
Homogeneity	0.31	0.04	0.32	0.05	0.31	0.04	0.518	0.624
GLRL features								
SRE	0.03	0.02	0.02	0.01	0.03	0.01	0.599	0.687
LRE	0.03	0.02	0.03	0.01	0.03	0.01	0.651	0.703
GLN	0.03	0.02	0.02	0.01	0.03	0.01	0.622	0.696
RLN	0.03	0.02	0.03	0.01	0.03	0.01	0.673	0.703
RP	189.29	42.68	174.70	45.80	179.20	51.34	0.317	0.395
LGRE	189.21	43.17	174.50	46.30	178.83	51.93	0.307	0.395
HGRE	189.98	42.61	175.60	45.30	180.32	51.19	0.312	0.395
SRLGE	189.02	43.21	174.30	46.30	178.87	51.66	0.319	0.395
SRHGE	377.40	357.20	573.60	406.50	494.00	514.39	**0.016***	0.071
LRLGE	404.07	373.94	612.40	435.20	537.90	556.81	**0.019***	0.071
LRHGE	331.56	298.09	502.00	366.90	438.90	458.96	**0.023***	0.072
GLGM features								
MGR	3.24	1.49	4.21	1.93	3.45	1.88	**0.027***	0.075
VGR	12254.33	5350.48	15694.81	6995.08	12975.09	7119.37	**0.043***	0.101
Skewness	41.49	7.95	36.15	7.75	39.39	11.24	**0.012***	0.071
Kurtosis	1878.42	684.14	1453.51	650.77	1773.01	885.30	**0.012***	0.071
Laws features								
L1	8.63e5	3.03e5	6.66e5	2.10e5	6.39e5	3.09e5	**0.021***	0.071
L2	1.92e5	1.55e5	1.35e5	6.38e4	1.32e5	7.32e4	0.174	0.256
L3	4.28e4	1.63e4	3.42e4	1.27e4	3.30e4	1.65e4	0.090	0.143
L4	2.13e5	9.97e4	1.61e5	5.63e4	1.56e5	7.22e4	**0.037***	0.092
L5	6.56e4	3.64e4	4.98e4	2.54e4	4.54e4	2.71e4	0.091	0.143
L6	4.35e4	2.20e4	3.26e4	1.80e4	3.03e4	1.96e4	0.091	0.143
L7	2.56e4	1.09e4	1.97e4	7.94e3	1.89e4	1.02e4	0.072	0.134
L8	1.01e5	5.70e4	7.17e4	4.17e4	6.72e4	4.85e4	0.078	0.136
L9	9.61e4	3.30e4	7.95e4	2.63e4	7.57e4	3.57e4	0.074	0.134
Mean Laws	8.23e5	3.31e5	8.55e5	2.14e5	7.62e5	3.25e5	0.565	0.664
Chi-square features								
Variance	16.17	7.86	20.49	7.42	16.02	9.59	**0.017***	0.071
VGR	6.38	2.58	7.78	2.60	7.05	3.89	**0.034***	0.089

*Statistically significant ($P < 0.05$, $Q < 0.05$). SD indicates standard deviation; IQR, interquartile range; GLCM, gray-level co-occurrence matrix features; GLRL, gray-level run-length features; SRE, short-run emphasis; LRE, long-run emphasis; GLN, gray-level nonuniformity; RLN, run-length nonuniformity; RP, run percentage; LGRE, low gray-level run emphasis; HGRE, high gray-level run emphasis; SRLGE, short-run low gray-level emphasis; SRHGE, short-run high gray-level emphasis; LRLGE, long-run low gray-level emphasis; LRHGE, long-run high gray-level emphasis; GLGM, gray-level gradient matrix features; MGR, mean gradients; VGR, variance gradient.

the study are shown in Table 1. The posterior mandibular region was the location most frequently encountered in all lesions. About 38% (14/37) of OKCs and 21% (4/19) of the AMs included the tooth crowns of impacted teeth similar to DCs. Septae were not detected in approximately 70% (26/37) of the OKCs and 42% (8/19) of AMs, similar to DCs.

3.2. Texture features and statistical analysis

The segmented volumes were shown in Table 1. Overall, the segmented volume of DCs tended to be smaller than OKCs and AMs. The values of texture features and results of Kruskal-Wallis nonparametric analysis are shown in Table 2. The texture analysis revealed that 9 histogram features, 1 GLCM feature, 3 GLRL features, 4 GLGM features, 2 Laws features, and 2 Chi-square features showed significant

Table 3
Analysis of the texture features with significant difference on Kruskal-Wallis test using Mann-Whitney's U test.

	DC vs. OKC		AM vs. OKC		AM vs. DC	
Texture features	*P*-value	*Q*-value	*P*-value	*Q*-value	*P*-value	*Q*-value
Histogram features						
Mean	**0.010***	**0.029***	**0.013***	0.176	0.528	0.786
Median	**0.008***	**0.029***	**0.013***	0.176	0.570	0.786
SD	**0.007***	**0.029***	0.426	0.871	0.121	0.355
2nd SD	**0.024***	0.053	0.755	0.910	0.088	0.355
SD5	**0.012***	**0.030***	0.917	0.958	**0.034***	0.355
Geometric mean	**0.009***	**0.029***	**0.015***	0.176	0.570	0.786
Harmonic mean	**0.010***	**0.029***	**0.015***	0.176	0.559	0.786
IQR	**0.001***	**0.029***	0.446	0.873	**0.041***	0.355
Fourth moment	**0.011***	**0.030***	0.678	0.910	0.075	0.355
GLCM features						
Entropy	**0.004***	**0.029***	0.151	0.608	0.646	0.821
GLRL features						
SRHGE	**0.003***	**0.029***	0.207	0.608	0.508	0.786
LRLGE	**0.004***	**0.029***	0.188	0.608	0.528	0.786
LRHGE	**0.005***	**0.029***	0.200	0.608	0.580	0.786
GLGM features						
MGR	**0.006***	**0.029***	0.156	0.608	0.895	0.895
VGR	**0.010***	**0.029***	0.194	0.608	0.821	0.858
Skewness	**0.002***	**0.029***	0.177	0.608	0.498	0.786
Kurtosis	**0.003***	**0.029***	0.151	0.608	0.549	0.786
Laws features						
L1	**0.009***	**0.029***	0.830	0.929	0.061	0.355
L4	**0.013***	**0.031***	0.943	0.964	0.121	0.355
Chi-square features						
Variance	**0.010***	**0.029***	**0.033***	0.259	0.809	0.858
VGR	**0.012***	**0.030***	0.100	0.608	0.761	0.845

*Statistically significant ($P < 0.05$, $Q < 0.05$). SD indicates standard deviation; IQR, interquartile range; GLCM, gray-level co-occurrence matrix features; GLRL, gray-level run-length features; SRHGE, short-run high gray-level emphasis; LRLGE, long-run low gray-level emphasis; LRHGE, long-run high gray-level emphasis; GLGM, gray-level gradient matrix features; MGR, mean gradients; VGR, variance gradient.

differences among the different types of lesions.

The results of Mann-Whitney's U test are shown in Table 3. Separated pairwise analysis revealed that 9 histogram features, 1 GLCM feature, 3 GLRL features, 4 GLGM features, 2 Laws features, and 2 Chi-square features showed significant differences between DC and OKC. Four histogram features and 1 Chi-square feature showed significant differences between OKC and AM. Two histogram features showed significant differences between DC and AM. After performing the FDR correction, 8 histogram features, 1 GLCM feature, 3 GLRL features, 4 GLGM features, 2 Laws features, and 2 Chi-square features between DC and OKC remained statistically significant. Representative examples of DCs, OKCs, and AMs are shown in Fig. 2.

4. Discussion

Texture analysis can extract mineable high-dimensional data from digital medical images and may aid in the identification and differentiation of various lesions [9–13], including those of the jaw [29]. For example, in one study texture analysis was used to identify and characterize cystic jaw lesions on digital panoramic radiographs with promising preliminary results [30]. In another study, a hybrid of surface and texture features from cone-beam CT were used to develop an automated classification of maxillofacial cysts that improved the performance of computer assisted diagnosis [31]. In our study, we evaluated the CT image texture features of DCs, OKCs, and AMs. After FDR analysis, we found 8 histogram, 1 GLCM feature, 3 GLRL features, 4 GLGM features, 2 Laws features, and 2 Chi-square features with significant differences between DCs and OKCs. To the best of our knowledge this is the first study that applied CT texture analysis to investigate cystic and cystic-appearing lesions in the jaw.

Cystic lesions of the jaw are readily apparent on radiographs or CT, however subtle differences in internal components within the lesions are often difficult to assess quantitatively. In this study, CT texture analysis was performed on the segmented internal components of selected lesions without including osseous septa. This was done to analyze the differences in texture parameters of the lesions' internal components, not the osseous structures. As the cystic components of the various lesions are inherently different pathologically, the texture features should also be different.

The cystic spaces of OKCs usually contain fluids with a comparatively lower soluble protein concentration [32]. However, several studies have suggested that the characteristic histologic finding of desquamated keratin sometimes present in OKCs contributes to subtle high density areas that when present on CT may allow differentiation from AMs [32–35]. We believe the differences between histogram features reflected the high density component in OKCs.

Other texture parameters such as GLCM, GLRL, GLGM, Laws features and Chi-square features showed significant differences when comparing DCs and OKCs. Pathologically, DCs contain fluid with or without inflammatory cells, cholesterol or hyaline bodies, and may not have a great impact on CT texture features. As described above, OKCs are comprised of keratin debris and fluid which may correspond to a highly complicated pattern of design on CT. We believe this difference was reflected in the results of our study.

Before the FDR analysis, some texture features showed significant differences between AMs and OKCs and between AMs and DCs. The multiple subtypes of AM may produce different densities on CT [33]. Histologically, in the plexiform type of AMs, cyst formation is usually the result of stromal degeneration [36], whereas in the follicular type, intercellular edema may cause cysts to coalesce and form large cavities. The cystic spaces in AMs usually also contain more proteinaceous fluid associated with colloidal materials. The relatively larger standard deviation of texture features of AMs compared with DCs or OKCs may be secondary to their inherent histological variability, and may be helpful to differentiate AMs from DCs and OKCs.

Texture analysis has the potential to prevent biopsies and expedite therapy. Biopsies are often problematic in OKCs, as inflammatory alterations may be so extensive that histological distinction from other cystic lesions is difficult without extensive additional tissue sampling to make the diagnosis [36]. Noninvasive tissue analysis with texture analysis can yield more information and prevent additional invasive procedures.

The widespread availability of CT compared with MR imaging makes CT texture analysis a very compelling technology. Although MR imaging may offer detailed information and soft tissue characterization in distinguishing OKCs from AMs by using differences in T1 and T2 signal intensity, contrast-enhancement, and apparent diffusion coefficients [38], the rising costs on health care and longer MR imaging exam time are not ideal.

This study has several limitations. Although a small cohort, the results of our analysis showed that texture features can discriminate OKCs from AMs and DCs from AMs by histogram features, and OKCs from DCs by utilizing other texture features. The lesions analyzed in this study included different subtypes of each tumor type. Dividing the tumors into their subgroups, such as uni-cystic or multi-cystic, could potentially affect the results. We examined the texture features of lesions imaged with unenhanced CT. Texture analysis of lesions imaged with contrast-enhanced CT images may provide additional information, especially in differentiating AMs which often have solid components. However, unenhanced CT is often the first-line imaging modality to evaluate cystic lesions of the jaw, and some patients may not be able to receive intravenous contrast due to impaired renal function or allergy

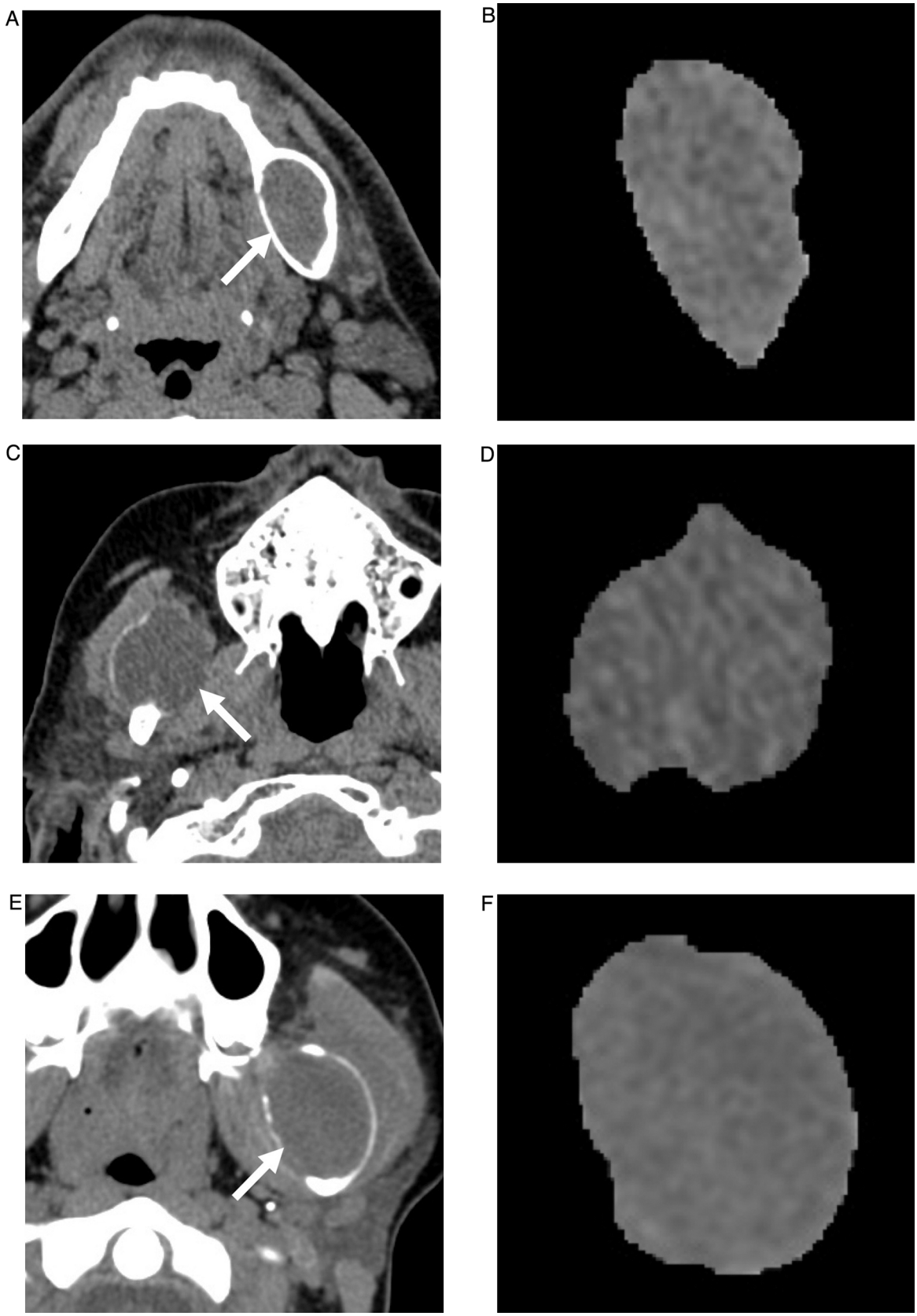

Fig. 2. Representative examples of the CT images (*A*, *C* and *E*) and corresponding segmented images (*B*, *D* and *F*) of each lesion. Dentigerous cyst in a 54-year-old man (*A* and *B*), odontogenic keratocyst in a 79-year-old woman (*C* and *D*), and ameloblastoma in a 17-year-old woman (*E* and *F*).

[37]. Finally, there may be limited generalizability of our results to CT protocols utilized at other institutions as differences in CT detector array configurations, acquisition mode, section thickness, kVp, mAs, and image reconstruction algorithms may affect texture features [39].

5. Conclusions

This pilot study demonstrates that differences in texture analysis features may help non-invasively differentiate several cystic lesions of the jaw. This study adds to the limited previously published data and suggests a potentially novel image-based assessment of odontogenic cystic and cystic-appearing lesions, which can be considered as an adjunct to the evaluation and diagnosis.

Funding sources

This research did not receive any specific grant from funding agencies in the public, commercial, or not-for-profit sectors

Source of funding

None.

Declaration of Competing Interest

None.

References

[1] M. Shear, The aggressive nature of the odontogenic keratocyst: is it a benign cystic neoplasm? Part 1. Clinical and early experimental evidence of aggressive behavior, Oral Oncol. 38 (2002) 219–226, https://doi.org/10.1016/S1368-8375(01)00065-3.
[2] T.P. Williams, F.A. Connor Jr., Surgical management of the odontogenic keratocyst: aggressive approach, J. Oral Maxillofac. Surg. 52 (1994) 964–966, https://doi.org/10.1016/S0278-2391(10)80081-3.
[3] R. Raitz, J.N. Assuncao Jr., L. Correa, et al., Parameters in panoramic radiography for differentiation of radiolucent lesions, J. Appl. Oral Sci. 17 (2009) 381–387, https://doi.org/10.1590/S1678-77572009000500006.
[4] B. Devenney-Cakir, R.M. Subramaniam, S.M. Reddy, et al., Cystic and cystic-appearing lesions of the mandible: review, AJR Am. J. Roentgenol. 196 (2011) WS66–77, https://doi.org/10.2214/AJR.09.7216.
[5] S.C. White, M.J. Pharoha, Cysts and cystlike lesions of the jaws, in: S.C. White, M.J. Pharoha (Eds.), Oral Radiology: Principles and Interpretation. 6th ed., Mosby Elsevier, St. Louis, 2009, pp. 343–365.
[6] S.J. Theodorou, D.J. Theodorou, D.J. Sartoris, Imaging characteristics of neoplasms and other lesions of the jawbones: part 1. Odontogenic tumors and tumorlike lesions, Clin. Imaging 31 (2007) 114–119, https://doi.org/10.1016/j.clinimag.2006.12.022.
[7] R.J. Scholl, H.M. Kellett, D.P. Neumann, et al., Cysts and cystic lesions of the mandible: clinical and radiologic-histopathologic review, Radiographics 19 (1999) 1107–1124, https://doi.org/10.1148/radiographics.19.5.g99se021107.
[8] K.E. Adebiyi, V.I. Ugboko, G.O. Omoniyi-Esan, et al., Clinicopathological analysis of histological variants of ameloblastoma in a suburban Nigerian population, Head Face Med. 2 (2006) 42, https://doi.org/10.1186/1746-160X-2-42.
[9] R.J. Gillies, P.E. Kinahan, H. Hricak, Radiomics: Images Are More than Pictures, They Are Data, Radiology 278 (2016) 563–577, https://doi.org/10.1148/radiol.2015151169.
[10] R.T. Larue, G. Defraene, D. De Ruysscher, et al., Quantitative radiomics studies for tissue characterization: a review of technology and methodological procedures, Br. J. Radiol. 90 (2017) 20160665, https://doi.org/10.1259/bjr.20160665.
[11] P. Kickingereder, S. Burth, A. Wick, et al., Radiomic profiling of glioblastoma: identifying an imaging predictor of patient survival with improved performance over established clinical and radiologic risk models, Radiology 280 (2016) 880–889, https://doi.org/10.1148/radiol.2016160845.
[12] Y. Huang, Z. Liu, L. He, et al., Radiomics signature: a potential biomarker for the prediction of disease-free survival in early-stage (I or II) non-small cell lung cancer, Radiology 281 (2016) 947–957, https://doi.org/10.1148/radiol.2016152234.
[13] R.A. Gatenby, O. Grove, R.J. Gillies, Quantitative imaging in cancer evolution and ecology, Radiology 269 (2013) 8–15, https://doi.org/10.1148/radiol.13122697.
[14] M. Zhou, J. Scott, B. Chaudhury, et al., Radiomics in brain tumor: image assessment, quantitative feature descriptors, and machine-learning approaches, AJNR Am. J. Neuroradiol. 39 (2018) 208–216, https://doi.org/10.3174/ajnr.A5391.
[15] X. Tang, Texture information in run-length matrices, IEEE Trans. Image Process. 7 (1998) 1602–1609, https://doi.org/10.1109/83.725367.
[16] R. Haralick, K. Shanmugam, I. Dinstein, Textural features for image classification, IEEE Trans. Syst. Man Cybern. A. Syst. Hum. 6 (1973) 610–621, https://doi.org/10.1109/TSMC.1973.4309314.
[17] V. Goh, B. Ganeshan, P. Nathan, et al., Assessment of response to tyrosine kinase inhibitors in metastatic renal cell cancer: CT texture as a predictive biomarker, Radiology 261 (2011) 165–171, https://doi.org/10.1148/radiol.11110264.
[18] K.A. Miles, B. Ganeshan, M.R. Griffiths, et al., Colorectal cancer: texture analysis of portal phase hepatic CT images as a potential marker of survival, Radiology 250 (2009) 444–452, https://doi.org/10.1148/radiol.2502071879.
[19] B. Ganeshan, V. Goh, H.C. Mandeville, et al., Non-small cell lung cancer: histopathologic correlates for texture parameters at CT, Radiology 266 (2013) 326–336, https://doi.org/10.1148/radiol.12112428.
[20] K. Buch, A. Fujita, B. Li, et al., Using texture analysis to determine human papillomavirus status of oropharyngeal squamous cell carcinomas on CT, AJNR Am. J. Neuroradiol. 36 (2015) 1343–1348, https://doi.org/10.3174/ajnr.A4285.
[21] A. Fujita, K. Buch, B. Li, et al., Difference between HPV-positive and HPV-negative non-oropharyngeal head and neck cancer: texture analysis eeatures on CT, J. Comput. Assist. Tomogr. 40 (2016) 43–47, https://doi.org/10.1097/RCT.0000000000000320.
[22] A. Fujita, K. Buch, M.T. Truong, et al., Imaging characteristics of metastatic nodes and outcomes by HPV status in head and neck cancers, Laryngoscope 126 (2016) 392–398, https://doi.org/10.1002/lary.25587.
[23] H. Kuno, M.M. Qureshi, M.N. Chapman, et al., CT Texture analysis potentially predicts local failure in head and neck Squamous cell carcinoma treated with chemoradiotherapy, AJNR Am. J. Neuroradiol. 38 (2017) 2334–2340, https://doi.org/10.3174/ajnr.A5407.
[24] A. Tsai, K. Buch, A. Fujita, et al., Using CT texture analysis to differentiate between nasopharyngeal cancer and age-matched adenoid controls, Eur. J. Radiol. 108 (2018) 208–214, https://doi.org/10.1016/j.ejrad.2018.09.012.
[25] H. Yu, K. Buch, B. Li, et al., Utility of texture analysis for quantifying hepatic fibrosis on proton density MRI, J. Magn. Reson. Imaging 42 (2015) 1259–1265, https://doi.org/10.1002/jmri.24898.
[26] K.I. Laws, Textured Image Segmentation, No. USCIPI-940 University of Southern California Los Angeles Image Processing INST, (1980).
[27] G. Castellano, L. Bonilha, L.M. Li, et al., Texture analysis of medical images, Clin. Radiol. 59 (2004) 1061–1069, https://doi.org/10.1016/j.crad.2004.07.008.
[28] B. Li, H. Jara, H. Yu, et al., Enhanced Laws textures: a potential MRI surrogate marker of hepatic fibrosis in a murine model, Magn. Reson. Imaging 37 (2017) 33–40, https://doi.org/10.1016/j.mri.2016.11.008.
[29] D.K. Veena, A. Jatti, R. Joshi, et al., Characterization of dental pathologies using digital panoramic X-ray images based on texture analysis, Conference Proceedings: Annual International Conference of the IEEE Engineering in Medicine and Biology Society Annual Conference (2017) 592–595 2017.
[30] A. Mol, S.M. Dunn, P.F. van der Stelt, Diagnosing periapical bone lesions on radiographs by means of texture analysis, Oral Surg. Oral Med. Oral Pathol. 73 (1992) 746–750, https://doi.org/10.1016/0030-4220(92)90022-I.
[31] F. Abdolali, R.A. Zoroofi, Y. Otake, et al., Automated classification of maxillofacial cysts in cone beam CT images using contourlet transformation and Spherical Harmonics, Comput. Methods Programs Biomed. 139 (2017) 197–207, https://doi.org/10.1016/j.cmpb.2016.10.024.
[32] L. Janse van Rensburg, C.J. Nortje, I. Thompson, Correlating imaging and histopathology of an odontogenic keratocyst in the nevoid basal cell carcinoma syndrome, Dentomaxillofac. Radiol. 26 (1997) 195–199, https://doi.org/10.1038/sj.dmfr.4600240.
[33] I. Crusoe-Rebello, C. Oliveira, P.S. Campos, et al., Assessment of computerized tomography density patterns of ameloblastomas and keratocystic odontogenic tumors, Oral Surg. Oral Med. Oral Pathol. Oral Radiol. Endod. 108 (2009) 604–608, https://doi.org/10.1016/j.tripleo.2009.03.008.
[34] K. Yoshiura, Y. Higuchi, Y. Ariji, et al., Increased attenuation in odontogenic keratocysts with computed tomography: a new finding, Dentomaxillofac. Radiol. 23 (1994) 138–142, https://doi.org/10.1259/dmfr.23.3.7530666.
[35] Y. Ariji, M. Morita, A. Katsumata, et al., Imaging features contributing to the diagnosis of ameloblastomas and keratocystic odontogenic tumours: logistic regression analysis, Dentomaxillofac. Radiol. 40 (2011) 133–140, https://doi.org/10.1259/dmfr/24726112.
[36] P.J. Slootweg, Lesions of the jaws, Histopathology 54 (2009) 401–418, https://doi.org/10.1111/j.1365-2559.2008.03097.x.
[37] P.K. Palkowitsch, S. Bostelmann, P. Lengsfeld, Safety and tolerability of iopromide intravascular use: a pooled analysis of three non-interventional studies in 132,012 patients, Acta Radiol. 55 (2014) 707–714, https://doi.org/10.1177/0284185113504753.
[38] M. Sumi, Y. Ichikawa, I. Katayama, et al., Diffusion-weighted MR imaging of ameloblastomas and keratocystic odontogenic tumors: differentiation by apparent diffusion coefficients of cystic lesions, AJNR Am. J. Neuroradiol. 29 (2008) 1897–1901, https://doi.org/10.3174/ajnr.A1266.
[39] K. Buch, B. Li, M.M. Qureshi, et al., Quantitative assessment of variation in CT parameters on texture features: pilot study using a nonanatomic phantom, AJNR Am, J. Neuroradiol. 38 (2017) 981–985, https://doi.org/10.3174/ajnr.A5139.